Sol–Gel Electrophoretic Deposition for the Growth of Oxide Nanorods**

By *Steven J. Limmer* and *Guozhong Cao**

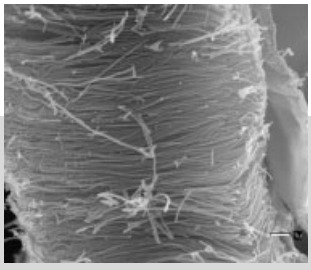

By combining sol–gel processing with electrophoretic deposition, we have developed a new method for the growth of oxide nanorods. Both single metal oxides (TiO_2, SiO_2) and complex oxides—$BaTiO_3$, $Sr_2Nb_2O_7$, and $Pb(Zr_{0.52}Ti_{0.48})O_3$—have been grown by this method. Uniformly sized nanorods 45–200 nm in diameter and 10 μm in length can be grown over large areas with near unidirectional alignment. The nanorods have the desired stoichiometric chemical composition and crystal structure, after firing to 500–700 °C for up to one hour.

1. Introduction

Metal oxides, particularly complex metal oxides, are important materials for various applications in industry and technology. They are used in such diverse areas as piezoelectrics for micro-electromechanical systems (MEMS) (typically lead zirconate titanate, PZT),[1] optically transparent electrodes in light-emitting diodes (such as tin oxide doped indium oxide (ITO)),[2] TiO_2 hybrid inorganic–organic photoelectrochemical cells,[3] and complex oxide catalysts and sensors.[4] In many of these applications, the sensitivity or efficiency is proportional to surface area. Nanorods or nanowires offer a larger surface area compared to that of films or the bulk material. Nanorods or nanowires also offer the opportunity to study the physical properties of one-dimensional structures. Numerous researchers have studied the synthesis and fabrication of nanorods and nanowires. Many different synthesis techniques have been developed, such as oxidation of metallic nanorods or nanowires,[5] vapor–liquid–solid (VLS) growth of oxide nanorods and nanowires,[6] and filling templates with sols or colloidal dispersions,[7,8] allowing the synthesis of many oxide nanorods. Of these techniques, the sol-filling method offers several advantages over both the VLS technique and oxidation of metallic nanorods or nanowires, and particularly facilitates the fabrication of complex oxide nanorods. However, the complete filling of solid inside the template holes could be challenging, considering the fact that typical sols or colloidal dispersions consist of 90 % or more solvent. In fact, the structures synthesized by this technique are often hollow tubes rather than solid rods.

We have developed an approach to synthesize and fabricate nanorods of complex oxides that combines several processing methods together, including sol–gel processing, electrophoretic deposition, and template-based growth. This method offers the possibility of making nanorods of any complex oxides, organic–inorganic hybrids and bio–inorganic hybrids. In addition, this technique allows the fabrication of unidirectionally aligned and uniformly sized nanorods with desired patterns for device fabrication, physical property measurements, and characterization.

2. Nanorods via Electrophoretic Deposition of Sols

Sol–gel processing is a wet chemical route for the synthesis and processing of inorganic and organic–inorganic hybrid materials. It is particularly useful in making complex metal oxides and temperature sensitive organic–inorganic hybrid materials. Typical sol–gel processing results in the formation of nanoscale particles of metal oxides. The particle size can be varied by changing the concentration and aging time.[9] In a typical sol, nanoparticles formed by hydrolysis and condensation reactions have a size ranging from 1 to 100 nm. These clusters are often stabilized electrostatically against agglomeration. Electrostatic stabilization is based on the surface charge of nanoparticles in a sol. Such a surface charge will interact with other charged species in the sol to form a charged structure around the particle, which in turn introduces an electric potential barrier to prevent two particles from approaching one another.

[*] S. J. Limmer, Prof. G. Z. Cao
Center for Nanotechnology
Department of Materials Science and Engineering
University of Washington
302 Roberts Hall, Box 352120 Seattle, WA 98195 (USA)
E-mail: gzcao@u.washington.edu

[**] SJL acknowledges (partial) support from the Joint Institute for Nanoscience funded by the Pacific Northwest National Laboratory (operated by Battelle for the U.S. Department of Energy) and the University of Washington.

  0935-9648/03/0503-0427 $ 17.50+.50/0

Upon application of an external electric field to a sol, the charged particles are set in motion in response to the electric field. This type of motion is referred to as electrophoresis. When a charged particle is in motion, some of the solvent surrounding the particle will move with it, since part of the solvent is tightly bound to the particle. The plane that separates the tightly bound liquid layer from the rest of the liquid is called the slip plane. The electric potential at the slip plane is known as the zeta potential. The zeta potential is determined by a number of factors, such as the particle surface charge density, the concentration of counter-ions in the solution, solvent polarity, and temperature. The mobility of a nanoparticle in a sol is dependent on the dielectric constant of the liquid medium, the zeta potential of the nanoparticle, and the viscosity of the solvent.

Electrophoretic deposition simply uses such an oriented motion of charged particles to grow films or monoliths by depositing the solid particles from a colloidal dispersion or a sol onto the surface of an electrode. If particles are positively charged (more precisely speaking, having a positive zeta potential), then the deposition of solid particles will occur at the cathode. Otherwise, deposition will be at the anode. At the electrodes, surface electrochemical reactions proceed to generate or receive electrons. The electrostatic double layers collapse upon deposition on the growth surface, and the particles coagulate. The films or monoliths grown by electrophoretic deposition from colloidal dispersions or sols are essentially a compaction of nanosized particles. Such films or monoliths are porous, i.e., there are voids inside. Typical packing densities, defined as the fraction of solid (also called green density) are less than 74 %, which is the highest packing density for uniformly sized spherical particles.[10] The green density of films or monoliths by electrophoretic deposition is strongly dependent on the concentration of particles in sols or colloidal dispersions, zeta potential, externally applied electric field, and reaction kinetics between particle surfaces. Slow reaction and slow arrival of nanoparticles at the surface would allow sufficient particle relaxation on the deposition surface, so that a high packing density is expected.

Many theories have been proposed to explain the processes at the deposition surface during electrophoretic deposition. Electrochemical process at the deposition surface or electrodes is complex and varies from system to system. However, in general, a current exists during electrophoretic deposition, indicating reduction and oxidation reactions occur at electrodes and/or deposition surface. In many cases, films or monoliths grown by electrophoretic deposition are electric insulators. However, the films or monoliths are porous and the surface of the pores would be electrically charged just like the nanoparticle surfaces, since surface charge is dependent on the solid material and the solution. Furthermore, the pores are filled with solvent or solution that contains counter-ions and charge-determining ions. The electrical conduction between the growth surface and the bottom electrode could proceed via either surface conduction or solution conduction. For the growth of nanorods, a porous template is used to restrict the deposition to occur inside the pores only.

Since films or monoliths grown by electrophoretic deposition are porous, post deposition sintering at elevated temperatures is usually required to form a dense material. However, considering the fact that the films or monoliths are a compaction of nanosized particles, sintering or densification is relatively easy compared to conventional ceramic sintering. If the initial solid particles were amorphous, sintering would also induce crystallization.

3. Oxide Nanorods by Sol–Gel Electrophoresis

A combination of sol–gel processing and electrophoretic deposition has been used to synthesize a variety of oxide nanorods, such as TiO_2, SiO_2, $BaTiO_3$, PZT, and $Sr_2Nb_2O_7$.[11,12] Figure 1 shows sample results obtained for TiO_2 nanorods. Scanning electron microscopy (SEM) images of three different sizes of TiO_2 nanorods grown in a polycarbonate membrane by sol–gel electrophoresis are shown. These nanorods have a uniform diameter throughout their entire length, with a surface that is smooth over much or all of the length. Comparing the various rods in each image, one can see that they all have roughly the same length and diameter. These images show that the rods are roughly parallel to one another over a large area. The diameters of the TiO_2 nanorods are estimated to be ~180 nm (for the 200 nm template), ~90 nm (for the 100 nm template), and ~45 nm (for the 50 nm template). This corresponds to approximately 10 % lateral shrinkage with respect to the membrane pore diameter. This size difference is most likely due to the volume shrinkage caused by densification during the heat treatment. Figure 1D shows a transmission electron microscopy (TEM) image of a TiO_2 nanorod, demonstrating that the nanorods are quite smooth and dense. Figure 1E shows a high-resolution TEM image and electron diffraction pattern, demonstrating that the nanorods are polycrystalline, with grains that are ~5 nm in size. An X-ray diffraction (XRD) spectrum of the TiO_2 rods is shown in Figure 1F, along with the spectrum for a powder formed from the same sol and fired at 500 °C for 60 min. From the powder XRD spectrum, it can be seen that the sample consists entirely of the anatase phase. Comparison of the two spectra shows that there are identical peaks in both samples. Further, the peak positions are the same and the intensity ratios among various peaks are similar. Note that there is a large amorphous background associated with the TiO_2 nanorods. This is due to the small volume of rods available for analysis, meaning that much of the X-ray beam was hitting the (amorphous) sample holder. For the TiO_2 rods grown in 50 nm templates, it was found that the drying time used has a strong influence on the durability of the nanorods. When the samples were dried at 100 °C for times up to 24 h, no nanorods were observed after firing at 500 °C. However, if the samples were dried for ~48 h prior to firing, nanorods were observed. It is likely that this result is due to the increased degree of condensation that occurred in the sample dried for a longer time. By allowing the samples to undergo further

  0935-9648/03/0503-0428 $ 17.50+.50/0

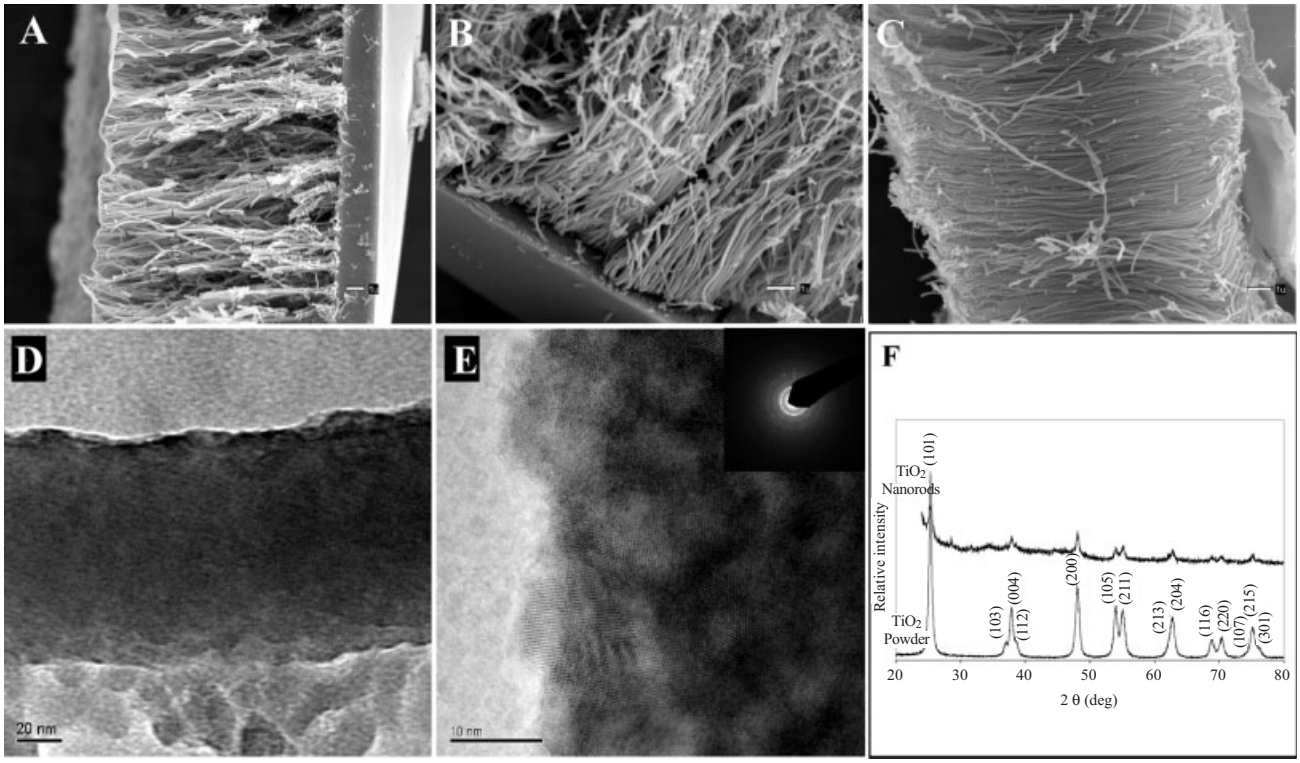

Fig. 1. SEM micrographs of different sizes of TiO_2 nanorods grown in a polycarbonate membrane by sol–gel electrophoresis. The diameters are approximately: A) ~180 nm (for the 200 nm template) diameter rods, B) ~90 nm (for the 100 nm template), and C) ~45 nm (for the 50 nm template). D) TEM micrograph of a TiO_2 nanorod, demonstrating that the nanorods are quite smooth and dense. E) High-resolution TEM image and electron diffraction pattern, demonstrating that the nanorods are polycrystalline, with grains of ~5 nm in size. F) XRD spectra of both the grown TiO_2 nanorods and a powder derived from the same sol. Both samples consist the anatase phase, and there is no observed shift in the peak positions for the nanorod sample. In addition, the relative intensities of the peaks are the same for the nanorod sample, showing that there is no preferred orientation in the sample.

condensation reactions, the rods formed were likely stronger, and thus better able to resist breakage upon firing.

Similar results have been obtained for $BaTiO_3$, SiO_2, $Sr_2Nb_2O_7$, and PZT nanorods grown by sol–gel electrophoresis.[12] The nanorods show shrinkages from ~0–37 % in diameter, have a relatively smooth surface, and are uniform in diameter throughout their entire length of ~10 μm. For a given composition, the nanorods all have roughly the same length and diameters, are formed over a broad area on the surface, and are arranged roughly parallel to one another. They also demonstrate the desired crystal phase as determined by XRD.

Upon application of an appropriate electric potential, the charged nanoparticles in the sol will be drawn towards the anode for SiO_2, and the cathode for the other oxides. The nanoparticles will fill the pores of the membrane, starting at the bottom, which is directly connected to the working electrode. In this manner, all the pores will eventually be completely filled. Prolonged deposition times lead to a layer of oxide forming on the membrane surface after the pores are filled. If we assume that the nanoparticles are uniformly sized spheres, then the highest possible packing density is 74 %.[10] This would also be the highest achievable density of the nanorods before densification. If there is a range of sizes in the nanoparticles, even denser packing could be possible. Upon heating the nanorods to an elevated temperature, densification will occur along with shrinkage. This explains why the observed diameter of the nanorods is smaller than that of the membrane pores. Although we do not know how closely the nanoparticles packed during the electrophoretic deposition, a lateral shrinkage of up to approximately 30 % was observed when the nanorods were fired. Since the times and temperatures used are sufficient to form fully dense films from these sols (except SiO_2), it is reasonable to assume that the nanorods are also fully dense after firing. This in turn implies that near ideal close packing of nanoparticles, for some systems such as TiO_2, might be achieved by this process.

The existence of broken nanorods in these figures could be explained as follows. The polycarbonate membrane templates burn off at approximately 400 °C in air, but the oxide nanorods are not likely to be fully dense (or crystallized) at this temperature, and thus have very limited mechanical strength. As the membrane and rods are heated, it is expected that some nanorods would break due to the differences in thermal expansion coefficients and distortion of the membranes. As noted earlier, the use of longer drying times induces a greater degree of condensation prior to firing of the samples. This in turn should make the samples stronger and more resistant to breakage during firing. This is being investigated in the formation of smaller TiO_2 nanorods, as well as the other oxide materials.

During nanorod growth, charged sol particles move due to electrophoresis towards the working electrode. They deposit

  0935-9648/03/0503-0429 $ 17.50+.50/0

at the bottom of the pore, while counter ions move in the opposite direction. As time increases, the densely packed sol particles fill more of the pore, until the pore is completely filled. Dense cross-sections of TiO_2 nanorods observed by SEM and TEM, shown in Figure 1, suggest that the growth of oxide nanorods does indeed follow this proposed mechanism.

The results presented so far clearly demonstrate the ability of the sol electrophoresis technique to form non-conductive nanorods. Beyond this, however, there is no kinetic information about the process by which nanorod formation occurs. Monitoring the current that flows in the growth cell during nanorod formation can yield some insights into the growth process and kinetics of the electrophoresis.

Figure 2A is a sample of the recorded current as a function of growth time for TiO_2 nanorods grown in a 100 nm template, with 5 V applied potential, and a spacing of 3 cm between the electrodes. From this data, one can see that the current rises quickly in the beginning of growth, and follows with a gradual increase after ~1500 s. It is postulated that the initial sharp current rise corresponds to the filling of the template pores from the bottom through the template. As the template pores are being filled with TiO_2 nanoparticles, the distance that charged species must move through the small template pores decreases. This results in a drop in the total resistance of the system, increasing the current. There is another possible mechanism leading to an increase in current due to the formation of a conductance path through the deposited TiO_2. Anatase is a wide bandgap semiconductor, and thus may conduct some of the current. It is possible that the resistivity of the deposited anatase is less than that of the anatase clusters moving in the sol, raising the current as the nanorods grow. After the pores are completely filled, the current rise with time is more gradual. This corresponds to the formation of a film of TiO_2 on top of the template.

To see how the data fits with the proposed growth model, it is useful to calculate the current vs time behavior assuming the model, to see if it fits with the observed data. The current was calculated using a method similar to that of Vandeperre and Van Der Biest,[13] where the current path was broken into three sections, as shown in Figure 3A. In each section, the resistance of the circuit is considered to consist of two parallel components. In section 1, the components are counter-ions diffusing through the pores of the TiO_2 deposit and conduction through the TiO_2 deposit. In sections 2 and 3, they are TiO_2 nanoparticles and counter-ions diffusing in the sol. Figure 3B shows the equivalent circuit used to calculate the current. The resistances are functions of the thickness of the template (s), the thickness of the deposit (d_l), and the distance between electrodes (d). They also

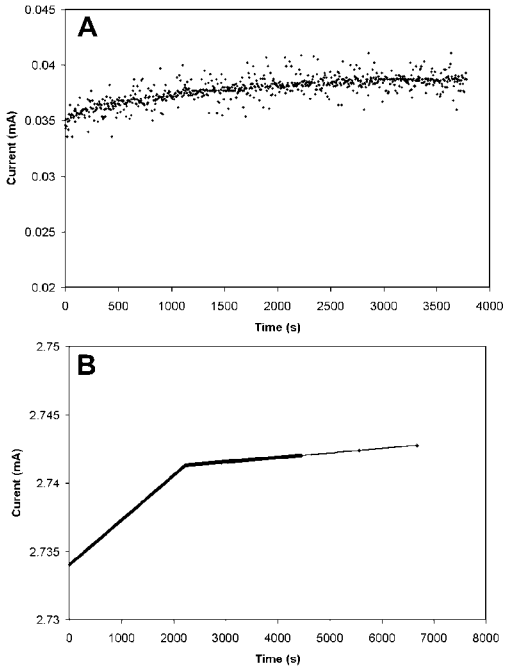

Fig. 2. A) A sample of the recorded current as a function of growth time for TiO_2 nanorods grown in a 100 nm template, with 5 V applied potential, and a spacing of 3 cm between the electrodes. B) A sample calculation of the current for TiO_2 grown in 100 nm templates at 5 V and 3 cm separating the electrodes.

depend on the cross-sectional area per template pore, the total number of pores, the cross-sectional area of the growth cell, the ionic resistivity of the sol, the resistivity of the TiO_2 deposit, the mobility of the TiO_2 nanoparticles, the effective charge per unit mass of the TiO_2 nanoparticles, and the con-

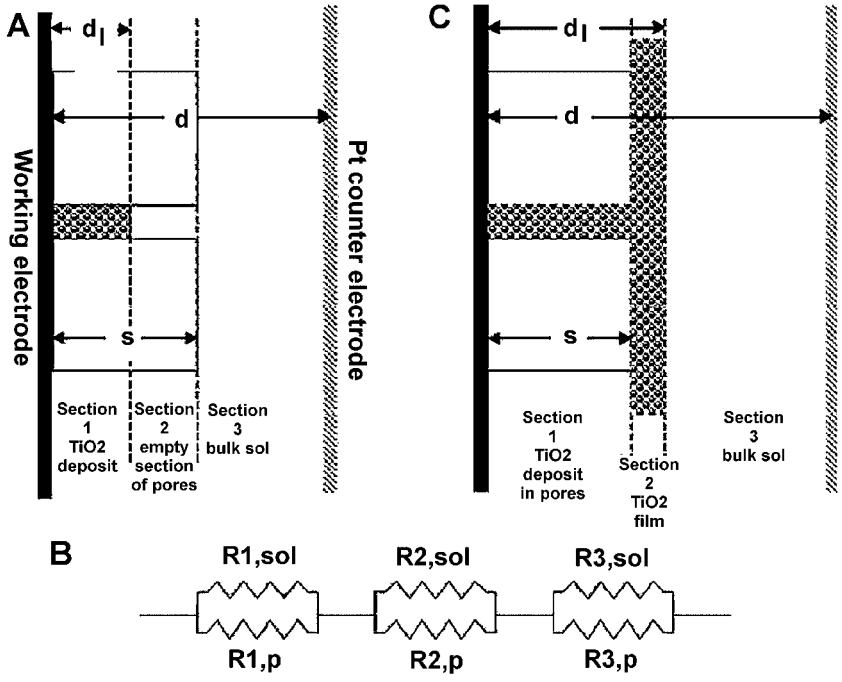

Fig. 3. The models used in calculation: A) the three sections of the growth process, for $d_l < s$, B) the equivalent circuit for (A), and C) the three sections of the growth process, for $d_l > s$.

  0935-9648/03/0503-0430 $ 17.50+.50/0

centration of the sol. Because of the small volume of TiO_2 depleted from the sol by nanorod growth (approximately ~1 % for the volume of sol used), the concentration of the sol is assumed to remain constant. In this circuit, the resistances due to the electrodes and the interface reactions are neglected, as they are likely to be constant with time.

This circuit only applies for times up to the moment when the template pores are completely filled; after that the system consists of three different sections as shown in Figure 3C. For this circuit, the resistances in sections 1 and 3 are similar to those above, modified for the fact that $d_1 > s$. However, in section 2 the resistances are similar to those in section 1, with the pore area replaced by the growth cell cross-sectional area.

Combining these resistances with the mass deposited as a function of time,[14] the volume of the deposit, and the voltage drop across the growth cell, it is possible to determine the growth current as a function of time. A plot of such a calculation is shown in Figure 2B for TiO_2 grown in 100 nm templates at 5 V with 3 cm separating the electrodes. While the currents calculated by this method are much larger than those measured, they show the identical qualitative trend. That is, the current increases sharply up to the time when the template pores are completely filled, and then increases more gradually as a film of TiO_2 forms over the entire template. It is observed that samples grown for longer times have a thick film attached to the nanorods, while those grown for shorter times have little or no film. Both experimental results and calculation strongly support the proposed model for the growth of non-conductive oxide nanorods by electrophoresis, in which nanorod growth proceeds via motion of the nanoparticles to the bottom of the template pores, filling them up as time proceeds.

4. Conclusions

The use of sol-electrophoresis with a template is a flexible method for synthesizing nanorods. In addition to the many materials we have synthesized, Miao et al[15] have recently demonstrated a modified version of this technique. They prepared single-crystalline TiO_2 nanowires by template-based electrochemically induced sol–gel deposition. Titania electrolyte solution was prepared using a method developed by Natarajan and Nogami,[16] in which Ti powder was dissolved into a H_2O_2 and NH_4OH aqueous solution, forming TiO^{2+} ionic clusters. When an external electric field was applied, TiO^{2+} ionic clusters diffused to the cathode and underwent hydrolysis and condensation reactions, resulting in depositing relative amorphous TiO_2 gel. After heat treatment in air at 240 °C for 24 h, nanowires of single-crystalline TiO_2 with anatase structure, diameters of 10, 20, and 40 nm, and lengths ranging from 2 to 10 μm were synthesized.

A number of possible applications exist for nanorods synthesized in the manner described in this paper. One example is current research we are conducting in fabricating TiO_2 nanorod photoelectrochemical cells. The higher surface area of nanorods and their relatively shorter conduction path should combine to make solar cells that are more efficient. Another application is the use of the higher surface area of nanorods for sensors, detectors, and catalysts. Patterned, ordered arrays of unidirectionally aligned nanorods could serve as the foundation of two-dimensional photonic bandgap crystals. Lastly, nanorods allow one to study the physical properties of one-dimensional structures.

[1] A. Kholkin, *Ferroelectrics* **2001**, *258*, 209.
[2] Y.-H. Tak, K.-B. Kim, H.-G. Park, K.-H. Lee, J.-R. Lee, *Thin Solid Films* **2002**, *411*, 12.
[3] E. Stathatos, P. Lianos, U. Lavrencic-Stangar, B. Orel, *Adv. Mater.* **2002,** *14*, 354.
[4] M. A. Peña , J. L. G. Fierro, *Chem. Rev.* **2001**, *101*, 1981.
[5] Y. Li, G. S. Cheng, L. D. Zhang, *J. Mater. Res.* **2000**, *15*, 2305.
[6] Z. W. Pan, Z. R. Dai, C. Ma, Z. L. Wang, *J. Am. Chem. Soc.* **2002**, *124*, 1817.
[7] B. B. Lakshmi, C. J. Patrissi, C. M. Martin, *Chem. Mater.* **1997**, *9*, 2544.
[8] B. Cheng, E. T. Samulski, *J. Mater. Chem.* **2001**, *11*, 2901.
[9] C. J. Brinker, G. W. Scherer, *Sol–gel science: the physics and chemistry of sol–gel processing*, Academic Press, San Diego, CA **1990.**
[10] W. D. Callister, *Materials science and engineering: an introduction*, John Wiley & Sons, New York **1997**.
[11] S. J. Limmer, S. Seraji, M. J. Forbess, Y. Wu, T. P. Chou, C. Nguyen, G. Z. Cao, *Adv. Mater.* **2001**, *13*, 1269.
[12] S. J. Limmer, S. Seraji, Y. Wu, T. P. Chou, C. Nguyen, G. Z. Cao, *Adv. Funct. Mater.* **2002**, *12*, 59.
[13] L. J. Vandeperre, O. O. Van Der Biest, *Innovative Processing and Synthesis of Ceramics, Glasses, and Composites*, American Ceramic Society, Westerville, OH **1997**, pp. 261–272.
[14] A. Simone, P. Spinelli, *Mater. Eng.* **2002**, *13*, 33.
[15] Z. Miao, D. Xu, J. Ouyang, G. Guo, Z. Zhao, Y. Tang, *Nano Lett.* **2002**, *2*, 717.
[16] C. Natarajan, G. Nogami, *J. Electrochem. Soc.* **1996**, *143*, 1547.

  0935-9648/03/0503-0431 $ 17.50+.50/0